Taylor & Francis
Taylor & Francis Group

Numerical Heat Transfer, Part B: Fundamentals

An International Journal of Computation and Methodology

ISSN: 1040-7790 (Print) 1521-0626 (Online) Journal homepage: www.tandfonline.com/journals/unhb20

A computational investigation of diffusivities and heat transfer in the flow of viscoelastic fluid through Darcy–Brinkman–Forchheimer medium

Anwar Shahid, Wang Wei, Tehseen Abbas & Muhammad Mubashir Bhatti

To cite this article: Anwar Shahid, Wang Wei, Tehseen Abbas & Muhammad Mubashir Bhatti (2025) A computational investigation of diffusivities and heat transfer in the flow of viscoelastic fluid through Darcy–Brinkman–Forchheimer medium, Numerical Heat Transfer, Part B: Fundamentals, 86:3, 762-779, DOI: 10.1080/10407790.2023.2296076

To link to this article: https://doi.org/10.1080/10407790.2023.2296076

NUMERICAL HEAT TRANSFER, PART B: FUNDAMENTALS
2025, VOL. 86, NO. 3, 762–779
https://doi.org/10.1080/10407790.2023.2296076

A computational investigation of diffusivities and heat transfer in the flow of viscoelastic fluid through Darcy–Brinkman–Forchheimer medium

Anwar Shahid[a], Wang Wei[b], Tehseen Abbas[b], and Muhammad Mubashir Bhatti[c,d]

[a]School of Science, Zhejiang University of Science and Technology, Hangzhou, P.R. China; [b]Department of Mathematics, Division of Science and Technology, University of Education, Lahore, Pakistan; [c]College of Mathematics and Systems Science, Shandong University of Science and Technology, Qingdao, P.R. China; [d]Material Science Innovation and Modelling (MaSIM) Research Focus Area, North-West University, Mmabatho, South Africa

ABSTRACT

The main objective of this work is to examine the effects of non-linear thermal radiation and induced magnetic fields on the behavior of viscoelastic fluid as it flows through a porous material that does not follow Darcy's law. Hence, the Darcy–Brinkman–Forchheimer model has been employed when formulating the momentum equation. The research postulates the presence of a chemical process involving two chemical species, *A* and *B*. The research utilizes the spectral relaxation method (SRM) for the numerical solution of the altered governing equations. The present algorithm is formulated and executed on computational software MATLAB. The findings demonstrate a high level of concurrence with previously known numerical outcomes in the context of a specific scenario. The findings of this research demonstrate that chemical species *B* functions as a catalyst in a horizontally subsurface environment. Consequently, the relationship between the homogeneous-heterogeneous scheme may be seen in the context of isothermal cubic autocatalytic events and first-order processes, respectively. The use of the heterogeneous reaction parameter offers significant benefits in reducing the concentration of the bulk fluid while increasing the concentration of the catalyst located on the subsurface. Moreover, the results indicate that the impacts of induced magnetic and viscoelastic factors on velocity and induced magnetic fields are similar in their outcomes but differ in their fundamental nature.

ARTICLE HISTORY

Received 20 September 2023
Revised 22 November 2023
Accepted 7 December 2023

KEYWORDS

Homogeneous–heterogeneous reactions; induced magnetic field; porous medium; spectral relaxation method (SRM); viscoelastic fluid

1. Introduction

It is well acknowledged that objects release thermal energy, and the intensity of this radiation is directly proportional to the temperature of the object. When two things with disparate temperatures are in close contact, thermal energy will flow from the item with a higher temperature to the one with a lower temperature until thermal equilibrium is reached. The assertion in question has been rigorously established as the fundamental principle of communication. This principle is widely recognized as the basis on which the modern theory of thermal radiation was developed throughout the nineteenth century.

CONTACT Muhammad Mubashir Bhatti mmbhatti@sdust.edu.cn; mubashirme@hotmail.com College of Mathematics and Systems Science, Shandong University of Science and Technology, Qingdao 266590, Shandong, P.R. China

The research conducted by Sandeep *et al.* [1] aims at investigating heat transfer in a magnetohydrodynamic (MHD) nanofluid as it flows over a shrinking or stretching surface. The study conducted by Zahor *et al.* [2] examined the effects of different parameters on entropy production, heat transfer, and velocity profiles in MHD flow of nanofluids. The objective of the research was to enhance the efficiency of thermodynamic systems. This work provides a comprehensive examination of the current body of literature pertaining to mathematical models that describe entropy formation in the context of magnetized fluid flow of nanofluids. A total of 141 journal articles published between 2010 and 2022 were reviewed, aiming to provide a thorough grasp of this research area. This work makes a valuable contribution to the advancement of thermodynamic systems by elucidating the utilization of mathematical models for entropy creation and furnishing essential insights for prospective investigations. It is worth mentioning that in some of the studies, the nonlinearity of temperature was mitigated by using Taylor series expansion, whereby higher-order terms were truncated. The process of simplification makes the nondimensionalization and parametrization of thermal radiation modeling a very simple task. However, it is important to acknowledge that the practicality of electromagnetic radiation in liquid during some industrial processes may not be evident when examined in a linear manner. Moreover, the Taylor series expansion is limited in its ability to provide comprehensive insights into the effects. Consequently, the incorporation of the nonlinear thermal radiation model has played a pivotal role in delivering precise elucidations. In a distinct relevant investigation, Animasaun [3,4] performed research on the dynamics of unsteady MHD flow and micropolar fluid flow through a vertically permeable subsurface. The study focused on the movement of binary mixes inside an optically sparse environment. The energy equation used in the research included radiative heat flux components that represented thermal radiation interactions within the fluid flow. These terms were written mathematically as a function of the temperature raised to the power of four. The dimensionless equations were derived in part using Taylor series expansion. The study conducted by Kothandapani and Prakash [5] investigated the influence of thermal radiation on the peristaltic transport in a tapered asymmetric geometry of MHD Williamson nanofluid. In a similar vein, Wakif *et al.* [6] reported their research findings on the thermo-physical properties of copper-water mixture in the presence of thermal radiation, specifically focusing on the behavior of small particles. The G-Chebyshev-G-Lob collocation technique was used to provide the numerical solution for the non-linear system of flow. The researchers documented an increase in the heat transfer ratio when the starting volumetric percentages of small particles and radiation parameters were increased. Numerous researchers have conducted investigations on the said topic and can be found from the list of references [7–10].

The study of fluid flow through a horizontally stretched subsurface has found practical applications in diverse industries, including pharmaceuticals (particularly medicinal pharmaceutical technologies), polyethylene and paper production, polymer extrusion, elastic sheet cooling, fiber technology, plastic material manufacturing, as well as in the fields of science and engineering technology. It is important to note that the bulk of the fluids described before exhibit both viscous and elastic characteristics when subjected to deformation. The investigation carried out by Cortell Bataller [11] focused on analyzing the heat transfer properties of a viscoelastic fluid as it flows from a stretched plate. The research specifically considered the implications of thermal radiation and viscous dissipation on these features. The research conducted by Singh and Agarwal [12] examined the impact of different thermal conductivity values on the behavior of a viscoelastic fluid as it flowed over an exponentially stretched subsurface. In their study, Abolbashari *et al.* [13] provided a detailed analysis of the characteristics of a non-Newtonian fluid in motion generated by a stretched surface. The study conducted by Adegbie *et al.* [14] examined the response of a micropolar fluid to a stagnation point on a deformable subsurface with continuous vortex viscosity. In a recent study, Sandeep *et al.* [15] conducted a comprehensive examination of the dual solutions associated with the governing equation that characterizes the stagnation-point flow in a

Jeffrey nanofluid across a stretched surface under the influence of an induced magnetic field and chemical reaction. Aly and Pop [16] performed a study on the MHD flow and heat transfer around the stagnation point of a surface undergoing either stretching or shrinking. The investigation takes into consideration the effects of partial slide and viscous dissipation. The evaluations of the stretched sheet have been further forth in references [17–21].

A chemical reaction occurs when two or more reactants combine to form a product. Autocatalysis is a phenomenon in which the products of a chemical process function as catalysts, therefore expediting the pace of chemical processes. In their study, Merkin [22] used the concept of order of magnitude and drew parallels to Ludwig Prandtl's assumptions on the application of Navier–Stokes equation at higher Reynolds numbers. Subsequently, he proposed a concise model to describe the interactions between homogeneous and heterogeneous reactants using two distinct chemical species, denoted as *A* and *B*. Chemically reactive fluid moving through a stretchy subsurface was examined by Mabood *et al.* [23]. The study conducted by Durairaj *et al.* [24] examined the characteristics of unsteady flow involving a Casson fluid across a vertical cone and flat plate that were saturated with a non-Darcy porous medium. The investigation considered factors, such as heat production or absorption and chemical interactions. This research employs numerical calculation and graphical visualizations to examine the impact of physical factors on the distributions of velocity, temperature, and concentration. The findings indicate that the Soret and Dufour effects have a substantial impact on the heat and mass transport properties, particularly in situations where there are considerable temperature and concentration gradients. In a study conducted by Animasaun [25], an investigation was conducted on the behavior of nth-order reactants in the context of Casson fluid flow, which includes the consideration of temperature-dependent plastic dynamic viscosity. Khan and Pop [26] conducted an analysis on the mechanisms involved in homogeneous-heterogeneous reactions occurring within the context of viscoelastic fluid flow. Eid *et al.* [27] conducted an examination on the analysis of the flow of electromagnetic radiative Prandtl fluid utilizing the Darcy-Forchheimer material scheme. Additionally, the study carried out by Zahir *et al.* [28] examined the consequences of nonlinear thermal radiation and homogeneous-heterogeneous interactions on the peristaltic movement of Johnson–Segalman fluid.

A porous medium may be defined as a composite material consisting of solid fibers that are interconnected by pores. The benefits of these types of media are derived from their increased interior surface area, which has been shown to be advantageous in insulation systems, thermal power technologies, and coating production processes. It is worth noting that the dissipation range of permeable medium is much greater than that of typical substrate coatings, leading to enhanced heat convection. Furthermore, the complex and complicated nature of porous materials makes them highly suitable for the process of filtration and controlling the flow of fluids, providing an exceptional means of regulating and enclosing ultimate actions. In order to further explore the intricacies of porous media, many researchers, including [29–33], have conducted investigations on several facets of these materials. The researchers used mathematical modeling methodologies, including the Darcy law and Dupuit–Forchheimer modeling, to investigate the effects of slip, magnetic fields, and heat production on hybrid nanofluids within their study. In addition, the authors conducted thermohydraulic assessments of salt-based nanofluids flowing through porous absorber tubes and emphasized the significance of using Darcy-Forchheimer models for entropy formation in the context of a nanofluid of third grade. In order to have a deeper understanding of porosity and the flow studies conducted using the Darcy-Forchheimer scheme, it is recommended to consult the relevant literature sources [34–37].

The fundamental goal of this research is to examine the flow behavior of a viscoelastic fluid near a deformable surface exposed to nonlinear thermal radiation. Furthermore, there has been not much research into the study of non-equilibrium diffusivities in the context of homogeneous-heterogeneous interactions in a viscoelastic fluid as it moves toward a stagnation point *via* a non-Darcian porous medium. The fluid flow in this study has been investigated by examining the momentum equation, energy equation, homogeneous-heterogeneous reaction model, and Darcy–Brinkman–Forchheimer model, and then transforming these equations into dimensionless form using relevant similarity variables. Using the Spectral Relaxation Method (SRM), the governing equations were successfully numerically solved. The primary benefit of the SRM method is its capacity to breakdown a complex set of equations into simpler subsystems, enabling incremental processing that is both computationally efficient and effective. The suggested approach of SRM has shown remarkable accuracy, simplicity in implementation, convergence, and efficiency when compared to existing numerical and analytical techniques [38–40] (such as *finite difference scheme* and *Runge–Kutta and Newton's method*) for addressing nonlinear problems. This study showcases the graphical and tabular depiction of the influence of dimensionless parametric values on several profiles, including velocity, induced magnetic field, temperature, and concentration. Additionally, the skin friction factor and local Nusselt number are also examined in this analysis.

2. Mathematical modeling

In the presence of an induced magnetic field and homogeneous-heterogeneous reactions, a steady electrically conductive viscoelastic fluid propagates toward a stagnation point and then along a horizontally stretched surface. The physical modeling, together with $\bar{x}$-axis and the $\bar{y}$-axis, is depicted in Figure 1. The stretchable surface is aligned with the $\bar{x}$-axis, while the $\bar{y}$-axis is perpendicular to it. The presence of an induced magnetic field seems to be essential due to the significant magnetic Reynolds number associated with the flow of viscoelastic fluids. The applicable magnetic field is granted a uniform strength of B_0. Additionally, an induced magnetic field is assumed to be exercised in the $\bar{y}$-direction, involving a parallel part approaching the numeric of $B_e = B_0$ in free-stream flow. Furthermore, the normal part elapses close to the wall. T_w and T_∞ are the temperatures adjacent and far away therefrom the stretched sheet. The stretchable and free-stream velocities are $\tilde{u}_w = c\bar{x}$ and $\tilde{u}_e = a\bar{x}$, where c and a are positive constants that nominate the stretched portion.

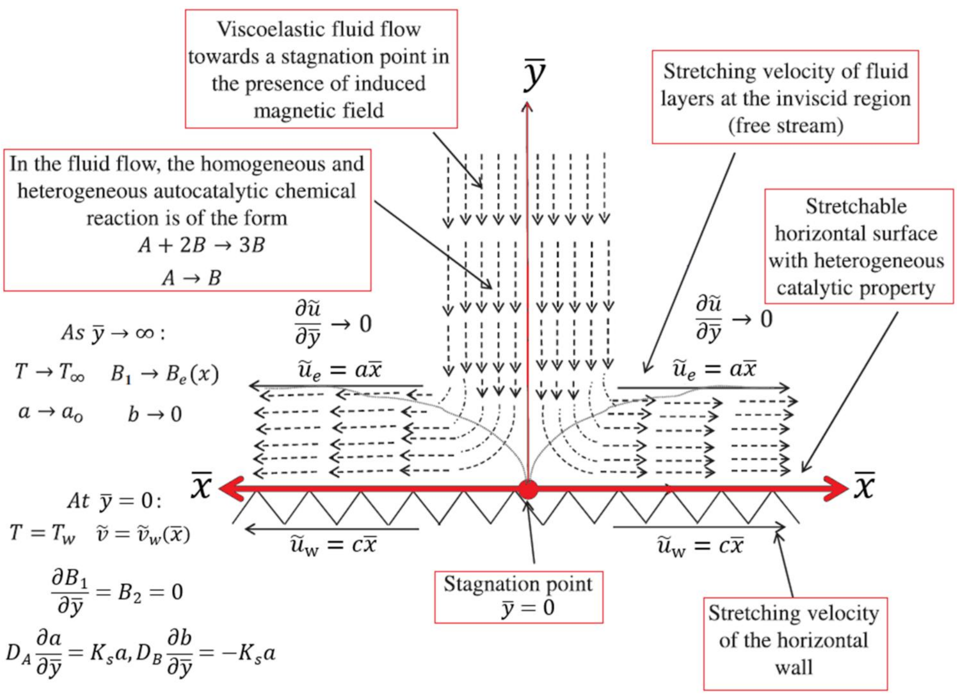

Figure 1. The physical structure of the viscoelastic fluid flows through a porous medium under the implications of induced magnetic field [43].

It is also presumed that a homogeneous-heterogeneous reactants exists amid A and B as the visco-elastic fluid flowing toward the stagnation-point and henceforth. This type of reaction is mentioned to as autocatalytic as specie B is claimed to be a catalyst. According to Merkin [22] supposition, that within the boundary layer, we have an isothermal cubic autocatalytic reaction specified by.

$$A + 2B \Rightarrow 3B, \ \text{rate} = K_c ab^2. \tag{1}$$

While the chemical reaction of the form takes place on the catalyst surface, it is a single, isothermal first-order reaction.

$$A \Rightarrow B, \ rate = K_s a. \tag{2}$$

The concentrations of species A and B are represented by a and b respectively. The reaction rate coefficients, k_c and k_s, cannot be counted as a constant since they include throughout parameters in common that may involve the reaction rate aside from concentration, that is clearly related in Eqs. (1) and (2). The governing equations for the boundary layer under the assumptions described above were derived by Merkin [22] and Ali *et al.* [41]:

$$\frac{\partial \tilde{u}}{\partial \overline{x}} + \frac{\partial \tilde{v}}{\partial \overline{y}} = 0, \tag{3}$$

$$\begin{aligned} \tilde{u}\frac{\partial \tilde{u}}{\partial \overline{x}} + \tilde{v}\frac{\partial \tilde{u}}{\partial \overline{y}} &= u_e \frac{\partial u_e}{\partial \overline{x}} + \frac{\mu}{\rho}\frac{\partial^2 \tilde{u}}{\partial \overline{y}^2} - \frac{k_0}{\rho}\left(\tilde{u}\frac{\partial^3 \tilde{u}}{\partial \overline{x}\partial \overline{y}^2} + \tilde{v}\frac{\partial^3 \tilde{u}}{\partial \overline{y}^3} + \frac{\partial \tilde{u}}{\partial \overline{y}}\frac{\partial^2 \tilde{v}}{\partial \overline{y}^2}\right) \\ &- \frac{\nu}{k}[\tilde{u} - u_e] - \frac{C_F}{\sqrt{k}}[\tilde{u} - u_e]^2 + \frac{\mu}{4\pi\rho}\left(B_1\frac{\partial B_1}{\partial \overline{x}} + B_2\frac{\partial B_1}{\partial \overline{y}} - B_e\frac{\partial B_e}{\partial \overline{x}}\right), \end{aligned} \tag{4}$$

$$\frac{\partial B_1}{\partial \overline{x}} = -\frac{\partial B_2}{\partial \overline{y}}, \tag{5}$$

$$\tilde{u}\frac{\partial B_1}{\partial \overline{x}} + \tilde{v}\frac{\partial B_1}{\partial \overline{y}} - B_1\frac{\partial \tilde{u}}{\partial \overline{x}} - B_2\frac{\partial \tilde{u}}{\partial \overline{y}} = \mu_e\frac{\partial^2 B_1}{\partial \overline{y}^2}, \tag{6}$$

$$\tilde{u}\frac{\partial T}{\partial \overline{x}} + \tilde{v}\frac{\partial T}{\partial \overline{y}} = \kappa\frac{1}{\rho c_p}\frac{\partial^2 T}{\partial \overline{y}^2} - \frac{1}{\rho c_p}\frac{\partial \tilde{Q}_r}{\partial \overline{y}}, \tag{7}$$

The current research introduces a modeling approach that combines homogeneous and heterogeneous reactants to examine the concentrations of substances A and B. These concentrations are determined by the reaction pattern represented by Eqs. (1) and (2):

$$\tilde{u}\frac{\partial a}{\partial \overline{x}} + \tilde{v}\frac{\partial a}{\partial \overline{y}} + K_c ab^2 = D_A\frac{\partial^2 a}{\partial \overline{y}^2}, \tag{8}$$

$$\tilde{u}\frac{\partial b}{\partial \overline{x}} + \tilde{v}\frac{\partial b}{\partial \overline{y}} - K_c ab^2 = D_B\frac{\partial^2 b}{\partial \overline{y}^2}. \tag{9}$$

Equations (3)–(9) are subject to boundary conditions and are expressed in the following form:

$$\begin{gathered} \tilde{u} = \tilde{u}_w(\overline{x}), \ \tilde{v} = \tilde{v}_w(\overline{x}), \ \frac{\partial B_1}{\partial \overline{y}} = B_2 = 0, \ T = T_w, \\ D_A\frac{\partial a}{\partial \overline{y}} = K_s a, \ D_B\frac{\partial b}{\partial \overline{y}} = -K_s a, \ \text{at } \overline{y} = 0 \\ \tilde{u} \to \tilde{u}_e(\overline{x}), \ \frac{\partial \tilde{u}}{\partial \overline{y}} \to 0, \ T \to T_\infty, \\ B_1 \to B_e = B_0\overline{x}, \ a \to a_0, \ b \to 0 \ \text{as } \overline{y} \to \infty \end{gathered} \tag{10}$$

It is worth noting that the magnetic permeability parameter for fluid μ_e is precisely amount to $^1/_{4\pi\sigma}$. In order to formulate the governing equations as a system of nonlinear ordinary differential equations (NODEs), the following similarity transformations are employed:

$$\left.\begin{array}{c}\tilde{u} = c\tilde{x}f'(\eta),\ \ \tilde{v} = -\sqrt{\nu c}f(\eta), \eta = \sqrt{\dfrac{c}{\nu}}\tilde{y},\ \ G(\eta) = \dfrac{a}{a_0}, H(\eta) = \dfrac{b}{a_0}, \\ B_1 = B_0\tilde{x}g'(\eta), \theta(\eta) = \dfrac{T - T_\infty}{T_w - T_\infty}, B_2 = -B_0\sqrt{\nu c}g(\eta)\end{array}\right\}, \tag{11}$$

The use of the Rosseland approximation technique in the analysis of thermal radiation enables the calculation of the heat flux associated with radiation:

$$\tilde{Q}_r = -\frac{4\overline{\sigma}}{3k^*}\frac{\partial T^4}{\partial \tilde{y}^4} = -\frac{16\overline{\sigma}}{3k^*}\frac{\partial}{\partial \tilde{y}}\{T \times T \times T \times T\} \tag{12}$$

whereas k^* and $\overline{\sigma}$ denote the Stefan–Boltzmann constant and mean absorption coefficient. It is further considered that temperature variances within the flow are not negligible. Therefore, simplifying the radiative heat flux by extending T^4 in a Taylor series to T_∞ and subsequently and do not consider higher-order components may not be a realistic approach. In order to simplify Eq. (12) and transform it into Eq. (7), one may use the technique of implicit differentiation.

$$\tilde{u}\frac{\partial T}{\partial \tilde{x}} + \tilde{v}\frac{\partial T}{\partial \tilde{y}} = \kappa\frac{1}{\rho c_p}\frac{\partial^2 T}{\partial \tilde{y}^2} + \frac{4\overline{\sigma}4T^3}{3k^*\rho c_p}\frac{\partial^2 T}{\partial \tilde{y}^2}, \tag{13}$$

If the relationship between $\theta_w = \frac{T_w}{T_\infty}$, is considered, it can be deduced that the similarity variable that pertains to the energy equation is identical to this value $T = \{1 + (\theta_w - 1)\theta\}T_\infty$.

The parameterization of the nonlinear component of heat radiation in Eq. (7) is notable since it is expressed in a novel way. Furthermore, the variables that are introduced in Eq. (11) satisfy Eqs. (3) and (5). By substituting Eq. (11) into Eqs. (3)–(10), we derive:

$$\begin{array}{c} f''' + \Gamma_1\left[ff^{iv} + f''^2 - f'''f'\right] - f'^2 + ff'' + M\left[g'^2 - gg'' - 1\right] - \beta_D f' \\ + \beta_D\lambda - F_r f'^2 - F_r\lambda^2 + 2\lambda F_r f' + \lambda^2 = 0, \end{array} \tag{14}$$

$$\varepsilon_1 g''' + fg'' - gf'' = 0, \tag{15}$$

$$\theta'' + {}^1/_R\{1 + (\theta_w - 1)\theta\}^3\theta'' + P_r f\theta' = 0, \tag{16}$$

$$G'' + Sc_A\left[fG' - K_0 GH^2\right] = 0, \tag{17}$$

$$\delta_1 H'' + Sc_B\left[fH' + K_0 GH^2\right] = 0. \tag{18}$$

In this study, we examine the case of a homogeneous-heterogeneous chemical reactants whereas the diffusion coefficients of A and B exhibit unequal diffusivities. As such, it is appropriate to preserve the dimensionless governing Eqs. (17) and (18). The boundary conditions take on as:

$$\begin{array}{c} f(\eta) = S,\ \ f'(\eta) = 1, g(\eta) = 0, g''(\eta) = 0, \theta(\eta) = 1, \\ G'(\eta) = K_s G,\ \ \delta_1 H'(\eta) = -K_s G,\ \text{ at } \eta = 0, \end{array} \tag{19}$$

$$\begin{array}{c} f'(\eta) \to \lambda,\ \ f''(\eta) \to 0, g'(\eta) \to 1, \theta(\eta) \to 0, \\ G(\eta) \to 1,\ \ H \to 0,\ \text{ as } \eta \to \infty. \end{array} \tag{20}$$

whereas

$$\left.\begin{array}{c} \Gamma_1 = \dfrac{k_0 c}{\rho\nu}, M = \dfrac{\mu B_0{}^2}{4c^2\rho\pi}, S = -\dfrac{\tilde{v}}{\sqrt{c\nu}}, \varepsilon_1 = \dfrac{\mu_e}{\nu}, R = \dfrac{3k^*\kappa}{16\overline{\sigma}T_\infty{}^3}, \\ P_r = \dfrac{\upsilon}{\alpha}, \beta_D = \dfrac{\nu}{ck}, F_r = \dfrac{C_F u_e}{a\sqrt{k}}, \lambda = \dfrac{a^2}{c^2}, Sc_A = \dfrac{\nu}{D_A}, Sc_B = \dfrac{\nu}{D_B}, \\ K_0 = \dfrac{K_c a_0{}^2}{c}, K_s = \dfrac{k_s}{D_A\sqrt{^c/_\nu}} \end{array}\right\} \tag{21}$$

where the viscoelastic parameter is symbolized as Γ_1, the magnetic parameter is symbolized as by M, the reciprocal magnetic Prandtl number is symbolized as ε_1, the Prandtl number is symbolized as P_r, the velocity proportion parametric quantity is symbolized as λ, the Schmidt numbers for chemical species A and B are symbolized as Sc_A, Sc_B, the strength of homogeneous and heterogeneous reactions are symbolized as K_0, K_s, and the suction parameter is symbolized as S, and the ratio of diffusion coefficient is symbolized as $\delta_1 = D_A/D_B$.

Physical parameters that are of interest in the field of engineering include the coefficient of shear stress, $Cf_{\bar{x}}$ (also known as the friction factor), and the local Nusselt number, $Nu_{\bar{x}}$. These values can be determined using the wall shear stress and heat flux, τ_w, q_w, which can be calculated as per the following equations.

$$Cf_{\bar{x}} = \frac{\tau_w}{\rho \tilde{u}_w{}^2}, Nu_{\bar{x}} = \frac{x q_w}{k(T_w - T_\infty)}, \tag{22}$$

$$\tau_w = \mu\left(\frac{\partial u}{\partial y}\right)_{y=0}, \quad q_w = -\kappa\left(\frac{\partial T}{\partial y}\right)_{y=0} \tag{23}$$

By utilizing the transformations referenced in Eq. (11), we can effectively derive the desired formulas:

$$\mathrm{Re}_{\bar{x}}^{\frac{1}{2}} Cf_{\bar{x}} = f''(0), \quad \mathrm{Re}_{\bar{x}}^{\frac{1}{2}} Nu_{\bar{x}} = -\theta'(0) \tag{24}$$

3. Numerical solutions

3.1. The SRM technique

The current set of non-linear ordinary differential equations (ODEs), namely Eqs. (14)–(18), together with the corresponding boundary conditions (19) and (20), are being analyzed using the SRM approach. The use of this methodology requires the reduction of the degree in the momentum Eq. (14). Letting that $f' = E$, Eqs. (14)–(18) take on the following form:

$$\begin{gathered} E'' + \Gamma_1\left[fE''' + E'^2 - EE''\right] - E^2 + fE' + M\left[g'^2 - gg'' - 1\right] - \beta_D E - F_r E^2 \\ +\beta_D \lambda - F_r \lambda^2 + 2\lambda F_r E + \lambda^2 = 0, \end{gathered} \tag{25}$$

$$\varepsilon_1 g''' + fg'' - gf'' = 0, \tag{26}$$

$$\theta'' + {}^1/_R\{1 + (\theta_w - 1)\theta\}^3 \theta'' + P_r f \theta' = 0, \tag{27}$$

$$G'' + Sc_A\left[fG' - K_0 G H^2\right] = 0, \tag{28}$$

$$\delta_1 H'' + Sc_B\left[fH' + K_0 G H^2\right] = 0. \tag{29}$$

The implementation of the Gauss–Seidel relaxation technique is used for the purpose of decoupling the contracted system in the following manner:

$$f'_{s+1} = E_s, \tag{30}$$

$$\begin{gathered} E''_{s+1} + \Gamma_1\left[f_s E'''_{s+1} + E'^2_s - E_s E''_s\right] - E^2_s + f_s E'_{s+1} + M\left[g'^2_s - g_s g''_s - 1\right] \\ -\beta_D E_{s+1} - F_r E^2_s + \beta_D \lambda - F_r \lambda^2 + 2\lambda F_r E_{s+1} + \lambda^2 = 0, \end{gathered} \tag{31}$$

$$\varepsilon_1 g'''_{s+1} + f_{s+1} g''_{s+1} - g_{s+1} f''_{s+1} = 0, \tag{32}$$

$$\theta''_{s+1} + {}^1/_R\{1 + (\theta_w - 1)\theta_s\}^3 \theta''_{s+1} + P_r f_{s+1} \theta'_{s+1} = 0, \tag{33}$$

$$G''_{s+1} + Sc_A\left[f_{s+1}G'_{s+1} - K_0 G_s H^2{}_s\right] = 0, \tag{34}$$

$$\delta_1 H''_{s+1} + Sc_B\left[f_{s+1}H'_{s+1} + K_0 G_{s+1}H^2{}_s\right] = 0. \tag{35}$$

The boundary conditions denoted by Eqs. (19) and (20) were subjected to a transformation.

$$\begin{gathered} f_{s+1}(0) = S,\ f'_{s+1}(0) = 1,\ g_{s+1}(0) = 0, g''_{s+1}(0) = 0, \theta_{s+1}(0) = 1, \\ G'_{s+1}(0) = K_s G_{s+1},\ \delta_1 H'_{s+1}(\eta) = -K_s G_{s+1}, \end{gathered} \tag{36}$$

$$f'_{s+1}(\infty) \to \lambda,\ f''_{s+1}(\infty) \to 0, g'_{s+1}(\infty) \to 1, \theta_{s+1}(\infty) \to 0, G_{s+1}(\infty) \to 1,\ H_{s+1}(\infty). \tag{37}$$

In this study, the recently approximated data is denoted by sub-components to indexing '$s+1'$', while the former approximated data is denoted by sub-components to indexing 's'. The Chebyshev pseudo-spectral method [42] is applied to Eqs. (30)–(37) at this stage. The computation of the differentiation matrix, denoted as '$D = {}^2/{}_l D$', is performed to estimate the magnitudes of the differentials of variables to be determined in Eqs. (30)–(37).

$$Df_{s+1} = E_s, \tag{38}$$

$$[\mathrm{diag}[a_{1,s}]D^3 + D^2 + \mathrm{diag}[a_{2,s}]D + \{-\beta_D + 2\lambda F_r\}I]E_{s+1} + \lambda^2 + \beta_D\lambda - F_r\lambda^2 - M = C_{1,s}, \tag{39}$$

$$[\varepsilon_1 D^3 + \mathrm{diag}[f_{s+1}]D^2 - \mathrm{diag}[f''_{s+1}]I]g_{s+1} = C_{2,s}, \tag{40}$$

$$\left[D^2 + P_r \mathrm{diag}[f_{s+1}]D\right]\theta_{s+1} = C_{3,s}, \tag{41}$$

$$\left[D^2 + Sc_A \mathrm{diag}[f_{s+1}]D\right]G_{s+1} = C_{4,s}, \tag{42}$$

$$\left[\delta_1 D^2 + Sc_B \mathrm{diag}[f_{s+1}]D\right]H_{s+1} = C_{5,s}. \tag{43}$$

The corresponding boundary conditions (36) and (37) transform:

$$\begin{gathered} f_{s+1}(\eta_N) = S,\ E_{s+1}(\eta_N) = 1,\ g_{s+1}(\eta_N) = g''_{s+1}(\eta_N) = 0, \theta_{s+1}(\eta_N) = 1, \\ G'_{s+1}(\eta_N) = K_s G_{s+1},\ \delta_1 H'_{s+1}(\eta_N) = -K_s G_{s+1} \end{gathered} \tag{44}$$

$$E_{s+1}(\eta_0) \to \lambda,\ E'_{s+1}(\eta_0) \to 0, g'_{s+1}(\eta_0) \to 1, \theta_{s+1}(\eta_0) \to 0, G_{s+1}(\eta_0) \to 1,\ H_{s+1}(\eta_0) \to 0. \tag{45}$$

Subsequently, the compressed form of Eqs. (38)–(43) is written as follows:

$$\ddot{\mathbf{A}}_1 f_{s+1} = \ddot{\mathbf{E}}_1, \tag{46}$$

$$\ddot{\mathbf{A}}_2 E_{s+1} = \ddot{\mathbf{E}}_2, \tag{47}$$

$$\ddot{\mathbf{A}}_3 g_{s+1} = \ddot{\mathbf{E}}_3, \tag{48}$$

$$\ddot{\mathbf{A}}_4 \theta_{s+1} = \ddot{\mathbf{E}}_4, \tag{49}$$

$$\ddot{\mathbf{A}}_5 G_{s+1} = \ddot{\mathbf{E}}_5, \tag{50}$$

$$\ddot{\mathbf{A}}_6 H_{s+1} = \ddot{\mathbf{E}}_6. \tag{51}$$

where

$$\begin{aligned}
&\ddot{\mathbf{A}}_1 = D,\ \ddot{\mathbf{E}}_1 = E_s, \\
&\ddot{\mathbf{A}}_2 = \mathrm{diag}[a_{1,s}]D^3 + D^2 + \mathrm{diag}[a_{2,s}]D + \{-\beta_D + 2\lambda F_r\}I + \left\{-M + \lambda^2 + \beta_D\lambda - F_r\lambda^2\right\}I,\ \ddot{\mathbf{E}}_2 = C_{1,s}, \\
&\ddot{\mathbf{A}}_3 = \varepsilon_1 D^3 + \mathrm{diag}[f_{s+1}]D^2 - \mathrm{diag}\left[f''_{s+1}\right]I,\ \ddot{\mathbf{E}}_3 = C_{2,s}, \\
&\ddot{\mathbf{A}}_4 = D^2 + P_r \mathrm{diag}[f_{s+1}]D,\ \ddot{\mathbf{E}}_4 = C_{3,s}, \\
&\ddot{\mathbf{A}}_5 = D^2 + Sc_A \mathrm{diag}[f_{s+1}]D,\ \ddot{\mathbf{E}}_5 = C_{4,s}, \\
&\ddot{\mathbf{A}}_6 = \delta_1 D^2 + Sc_B \mathrm{diag}[f_{s+1}]D,\ \ddot{\mathbf{E}}_6 = C_{5,s.}
\end{aligned}$$

and

$$a_{1,s} = \Gamma_1 f_s,\ \ a_{2,s} = f_s,\ \ C_{1,s} = (1 + F_r)E^2{}_s - \Gamma_1\left[E'^2{}_s - E_s E''{}_s\right] + M\left[g_s g''{}_s - g'^2{}_s\right],$$
$$C_{2,s} = 0,\ \ C_{3,s} = -{}^1/_R\{1 + (\theta_w - 1)\theta_s\}^3 D^2\theta_s,\ \ C_{4,s} = Sc_A K_0 G_s H^2{}_s, C_{5,s} = -Sc_B K_0 G_{s+1} H^2{}_s$$

whereas

$$\mathrm{diag}(a_{1,s}) = \begin{bmatrix} a_{1,s}(\eta_0) & \cdots & & \\ . & . & & . \\ . & & . & . \\ . & & & . \\ & \cdots & & a_{1,s}(\eta_N) \end{bmatrix},\ \mathrm{diag}(a_{2,s}) = \begin{bmatrix} a_{2,s}(\eta_0) & \cdots & & \\ . & . & & . \\ . & & . & . \\ . & & & . \\ & \cdots & & a_{2,s}(\eta_N) \end{bmatrix},$$

$$C_{1,s} = \begin{bmatrix} C_{1,s}(\eta_0) \\ . \\ . \\ . \\ C_{1,s}(\eta_N) \end{bmatrix}, C_{2,s} \begin{bmatrix} 0 \\ . \\ . \\ . \\ 0 \end{bmatrix} = C_{3,s} = \begin{bmatrix} C_{3,s}(\eta_0) \\ . \\ . \\ . \\ C_{3,s}(\eta_N) \end{bmatrix}, C_{4,s} = \begin{bmatrix} C_{4,s}(\eta_0) \\ . \\ . \\ . \\ C_{4,s}(\eta_N) \end{bmatrix}, C_{5,s} = \begin{bmatrix} C_{5,s}(\eta_0) \\ . \\ . \\ . \\ C_{5,s}(\eta_N) \end{bmatrix}.$$

$$f_{s+1} = \left[f(\eta_0), f(\eta_1), \ldots, f(\eta_N)\right]^T,\ \ E_{s+1} = \left[E(\eta_0), E(\eta_1), \ldots, E(\eta_N)\right]^T, g_{s+1} = \left[g(\eta_0), g(\eta_1), \ldots, g(\eta_N)\right]^T,$$
$$\theta_{s+1} = \left[\theta(\eta_0), \theta(\eta_1), \ldots, \theta(\eta_N)\right]^T,\ G_{s+1} = \left[G(\eta_0), G(\eta_1), \ldots, G(\eta_N)\right]^T,\ H_{s+1} = \left[H(\eta_0), H(\eta_1), \ldots, H(\eta_N)\right]^T$$

represents a set of vectors with dimensions $(\mathrm{N}+1)\times 1$, whereas 0 denotes a vector having dimensions of $(\mathrm{N}+1)\times 1$. Furthermore, I signifies the identity matrices having dimensions of $(\mathrm{N}+1)\times(\mathrm{N}+1)$.

The application of boundary conditions on the system of equations, as presented in Eqs. (46)–(51), is

$$\ddot{\mathbf{A}}_1 = \begin{bmatrix} & \ddot{\mathbf{A}}_1 & \\ \overline{0} & \overline{\cdots} & \overline{1} \end{bmatrix}, f_{s+1} = \begin{bmatrix} f_{s+1}(\eta_0) \\ f_{s+1}(\eta_1) \\ . \\ . \\ . \\ f_{s+1}(\eta_N) \end{bmatrix}, \ddot{\mathbf{E}}_1 = \begin{bmatrix} \ddot{\mathbf{E}}_1 \\ \overline{S} \end{bmatrix}, \ddot{\mathbf{A}}_2 = \begin{bmatrix} \frac{1}{D_{1,1}} & \frac{\cdots}{\cdots} & \frac{0}{D_{1,N}} \\ & \ddot{\mathbf{A}}_2 & \\ \overline{D_{N,1}} & \overline{\cdots} & \overline{D_{N,N}} \end{bmatrix}, E_{s+1} = \begin{bmatrix} \frac{E_{s+1}(\eta_0)}{E_{s+1}(\eta_1)} \\ . \\ . \\ . \\ \overline{E_{s+1}(\eta_N)} \end{bmatrix}, \ddot{\mathbf{E}}_2 = \begin{bmatrix} \frac{\lambda}{0} \\ \overline{1} \end{bmatrix},$$

$$\ddot{\mathbf{A}}_3 = \begin{bmatrix} \overline{D_{1,1}} & \frac{\cdots}{} & \overline{D_{1,N}} \\ & \ddot{\mathbf{A}}_3 & \\ \overline{D^2{}_{N,1}} & \cdots & \overline{D^2{}_{N,N}} \\ \overline{0} & \overline{\cdots} & \overline{1} \end{bmatrix}, g_{s+1} = \begin{bmatrix} \frac{g_{s+1}(\eta_0)}{g_{s+1}(\eta_1)} \\ . \\ . \\ . \\ \overline{g_{s+1}(\eta_N)} \end{bmatrix}, \ddot{\mathbf{E}}_3 = \begin{bmatrix} 1 \\ \frac{0}{0} \end{bmatrix}, \ddot{\mathbf{A}}_4 = \begin{bmatrix} \frac{1}{} & \frac{\cdots}{} & \frac{0}{} \\ & \ddot{\mathbf{A}}_4 & \\ \overline{0} & \overline{\cdots} & \overline{1} \end{bmatrix}, E_{s+1} = \begin{bmatrix} \frac{\theta_{s+1}(\eta_0)}{\theta_{s+1}(\eta_1)} \\ . \\ . \\ . \\ \overline{\theta_{s+1}(\eta_N)} \end{bmatrix}, \ddot{\mathbf{E}}_2 = \begin{bmatrix} \frac{0}{} \\ \ddot{\mathbf{E}}_2 \\ \overline{1} \end{bmatrix},$$

$$\ddot{\mathbf{A}}_5 = \begin{bmatrix} \frac{1}{} & \frac{\cdots}{} & \frac{0}{} \\ & \ddot{\mathbf{A}}_5 & \\ D_{N,1} & \cdots & D_{N,N} \end{bmatrix}, G_{s+1} = \begin{bmatrix} \frac{G_{s+1}(\eta_0)}{G_{s+1}(\eta_1)} \\ . \\ . \\ . \\ \overline{G_{s+1}(\eta_N)} \end{bmatrix}, \ddot{\mathbf{E}}_5 = \begin{bmatrix} \frac{1}{} \\ \ddot{\mathbf{E}}_5 \\ 0 \end{bmatrix}, \ddot{\mathbf{A}}_6 = \begin{bmatrix} \frac{1}{} & \frac{\cdots}{} & \frac{0}{} \\ & \ddot{\mathbf{A}}_5 & \\ \overline{D_{N,1}} & \overline{\cdots} & \overline{D_{N,N}} \end{bmatrix}, H_{s+1} = \begin{bmatrix} \frac{H_{s+1}(\eta_0)}{H_{s+1}(\eta_1)} \\ . \\ . \\ . \\ \overline{H_{s+1}(\eta_N)} \end{bmatrix}, \ddot{\mathbf{E}}_6 = \begin{bmatrix} \frac{0}{} \\ \ddot{\mathbf{E}}_6 \\ \overline{1} \end{bmatrix}.$$

The selected initial approximations presented as

$$\begin{gathered} f_0(\eta) = S + \lambda\eta + (1-\lambda)[1 - e^{-\eta}], E_0(\eta) = \lambda + (1-\lambda)e^{-\eta}, \\ E_0(\eta), g_0(\eta) = , \eta, \theta_0(\eta) = e^{-\eta} \\ G_0(\eta) = 1 - e^{-\eta} + \frac{1}{(K_s+1)}e^{-\eta}, H_0(\eta) = \frac{-K_s}{\delta_1(K_s+1)}e^{-\eta}. \end{gathered} \tag{52}$$

above adhere to the prescribed boundary conditions (44) and (45) and facilitate iterative refinement of the approximations for $f_s, E_s, g_s, \theta_s, G_s, H_s$, for all $s = 1, 2, 3, \ldots$ using the SRM methodology.

4. Results and discussion

This section examines the efficacy of pertinent parameters on the velocity $f'(\eta)$, induced magnetic field $g'(\eta)$, temperature $\theta(\eta)$, and concentration profiles $G(\eta)$ and $H(\eta)$. The results are presented through tables and graphs. Validation of the findings is depicted in Table 1, which showcases the agreement of $Cf_{\bar{x}}$ and $Nu_{\bar{x}}$ values with formerly published outcomes by Ali *et al.* [41], with favorable results across varying M. This further establishes the accuracy of the employed numerical algorithm. An exceptional agreement has been achieved, which attests to an improved convergence of the proposed approach. Tables 2 and 3 provide a numerical comparison of the values of $f''(0), f'''(0), g''(0), H'(0), G'(0)$ under the conditions of $\beta_D = F_r = 0$, while keeping the other parameters constant. It is worth mentioning that the current findings not only demonstrate accuracy, but also indicate that the SRM methodology is a more dependable and effective approach in comparison to other approaches [43]. Table 4 presents the numerical findings of $f''(0)$ and $g''(0)$ for the various collocation points 'N' in the SRM code, across M and Γ_1, while keeping all other parameters fixed. Notably, the results demonstrate a remarkable stability for different collocation point numbers N. It should be observed that, with increasing Γ_1, there is a considerable rise in $f''(0)$ and $g''(0)$. Furthermore, an augmented M, leads to a significant decline in $f''(0)$ and $g''(0)$, indicating a considerable retardation of boundary layer flow that is toward the stretching surface with intense employed magnetic field.

The impact of M on the longitudinal velocity $f'(\eta)$, and $g'(\eta)$ profiles of the flow are presented in Figures 2 and 3. It is evident that an increment in (M) results in a depreciation of both $f'(\eta)$, and $g'(\eta)$ profiles. The observed decrement in these figures can be attributed to the entity of the Lorentz force. As the parameter M grows in magnitude, the Lorentz force takes precedence and tends to amplify the viscous forces. This, in turn, brings to a reduction in $f'(\eta)$. The impact of the viscoelastic parameter (Γ_1 and S) on $f'(\eta)$, and $g'(\eta)$ profiles for the flow is depicted in Figures 4 and 5. The findings demonstrate that an escalation in (Γ_1) results in decrement in both

Table 1. The present estimations of $f''(0)$ and $-\theta'(0)$ were compared with the preceding investigation through the parameter M with fixation of $\lambda = 3$, $\Gamma_1 = 0, \beta_D = F_r = 0, R = \theta_w = 0$.

M	$f''(0)$	Ali *et al.* [41]	$-\theta'(0)$	Ali *et al.* [41]
0.1	4.70928	4.70927	0.97902	0.97902
0.5	4.62767	4.62765	0.97961	0.97961
1	4.52159	4.52158	0.97240	0.97240

Table 2. Numerical comparison with previous results for $f''(0), f'''(0)$ and $g''(0)$ for different values of M and Γ_1 and fixing the other parameters $\lambda = 0.8$, $\varepsilon_1 = 0.1, \beta_D = F_r = 0, R = 1, \theta_w = 1.01, P_r = 0.72$, $\delta_1 = 1.2$, $Sc_A = Sc_B = 0.62, K_0 = 1, K_s = 1$, and $S = 0.5$.

M	$f''(0)$	$g''(0)$	$f'''(0)$	$f''(0)$	$g''(0)$	$f'''(0)$
	Animasaun *et al.* [43]			Present results		
	$\Gamma_1 = 3$					
1	−0.076563	1.155076	0.002769	−0.076563	1.155076	0.002769
2	−0.147728	1.131197	0.088140	−0.147728	1.131197	0.088140
3	−0.191399	1.118931	0.156035	−0.191399	1.118931	0.156035
Γ_1	$M = 3$					
1	−0.315704	1.093213	0.419162	−0.315704	1.093213	0.419162
2	−0.227888	1.109898	0.218492	−0.227888	1.109898	0.218492
3	−0.191399	1.118931	0.156035	−0.191399	1.118931	0.156035

Table 3. Numerical comparison with previous results for $f''(0), f'''(0)$ and $g''(0)$ for different values of M and Γ_1 and fixing the other parameters $\lambda = 0.8$, $\varepsilon_1 = 0.1, \beta_D = F_r = 0, R = 1, \theta_w = 1.01, P_r = 0.72$, $\delta_1 = 1.2$, $Sc_A = Sc_B = 0.62$, and $S = 0.5$.

K_0	$G'(0)$	$H'(0)$	$G'(0)$	$H'(0)$
	Animasaun *et al.* [43]		Present results	
		$K_s = 1$		
1	0.43296989	−0.36080824	0.43296989	−0.36080824
2	0.42197286	−0.35164405	0.42197286	−0.35164405
3	0.41414673	−0.34512228	0.41414673	−0.34512228
K_s		$K_0 = 1$		
1	0.43296989	−0.36080824	0.43296989	−0.36080824
2	0.55214357	−0.46011964	0.55214357	−0.46011964
3	0.60884911	−0.50737425	0.60884911	−0.50737425

Table 4. The SRM solution's values for $f''(0)$ and $g''(0)$ for distinct M and Γ_1 with fixation of $\lambda = 0.8$, $\varepsilon_1 = 0.1, \beta_D = F_r = 0, R = 1, P_r = 0.72$, and $\theta_w = 1.01$.

N	Γ_1	M	$f''(0)$	$g''(0)$
50	3	1	−0.076542	1.155054
60	3	1	−0.076553	1.155064
70	3	1	−0.076563	1.155076
90	3	1	−0.076563	1.155076
50	3	2	−0.147706	1.131175
60	3	2	−0.147717	1.131186
70	3	2	−0.147728	1.131197
90	3	2	−0.147728	1.131197
50	1	3	−0.315681	1.093191
60	1	3	−0.315692	1.093202
70	1	3	−0.315704	1.093213
90	1	3	−0.315704	1.093213
50	2	3	−0.227865	1.109876
60	2	3	−0.227877	1.109887
70	2	3	−0.227888	1.109898
90	2	3	−0.227888	1.109898

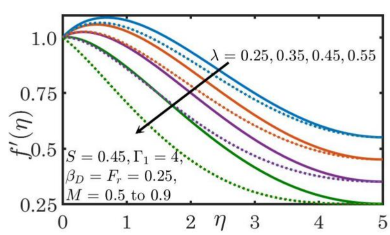

Figure 2. Variation of M and λ on $f'(\eta)$.

velocity profiles. The reason for this phenomenon can be elucidated by the increase in the visco-elastic parameter, causing a stronger adhesion of the hydrodynamic boundary layer to the surface. By enlarging the parameter S results in a deceleration of the convection capacity, both in the vicinity of and distant from the heated surface. This, in turn, results in a deceleration of the flow in both $f'(\eta)$, and $g'(\eta)$, as demonstrated in Figures 4 and 5. Figure 6 displays the impact of β_D and F_r on velocity magnitudes. The velocity decreases as the Momentum boundary layer thickness increases, which enhances both parameters since the flow decelerates. In Eq. (14), the permeable parameter $\beta_D = \frac{\nu}{ck}$ emerges in the form of the Darcian term $' - \beta_D f''$, a drag force linked to bulk porous medium fibers. The realistic permeability of the permeable medium, k, is inversely proportional to this term. As β_D increases, the permeability decreases, producing larger solid fiber resistance across viscoelastic fluid, resulting deceleration in $f'(\eta)$. The influence of

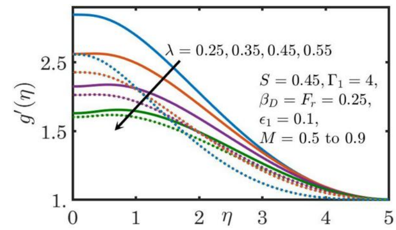

Figure 3. Variation of M and λ on g'.

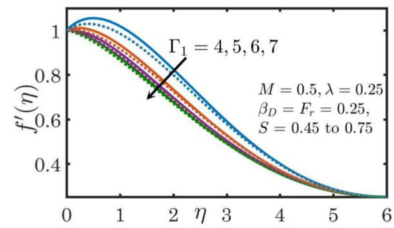

Figure 4. Effects for Γ_1 and S on $f'(\eta)$.

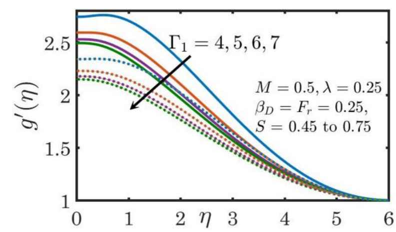

Figure 5. Variation of Γ_1 and S on g'.

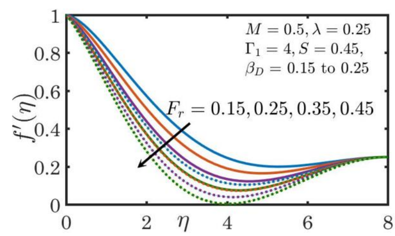

Figure 6. Influence of F_r and β_D on velocity distribution.

Forchheimer parameter F_r results in impressive retardation in $f'(\eta)$ for larger F_r. Figure 7 investigates the effects of ε_1 and λ on the induced magnetic field. It was observed that the $g'(\eta)$ field experiences a decrease in proximity to the boundary, while increasing further away with an increment into ε_1. Additionally, the velocity of the induced magnetic field, represented as $g'(\eta)$, experiences a reduction with an increase in λ within the vicinity of the wall. This is subsequently followed by a negligible increment.

The impact of R and λ, θ_w and P_r over the temperature function $\theta(\eta)$ are illustrated in Figures 8 and 9. The $\theta(\eta)$ experiences a reduction with respect to both parameters, i.e. by enlarging the numeric of R and λ. The R is observed to significantly slowdown the temperature in the flow range. Thermal radiation is recognized as a mechanism of energy transferal by the emission of electromagnetic waves that hold heat energy apart as the fluid flowing. As R increases, the ratio at which heat energy is set free from the flow range increases, thereby leading to a decrease in

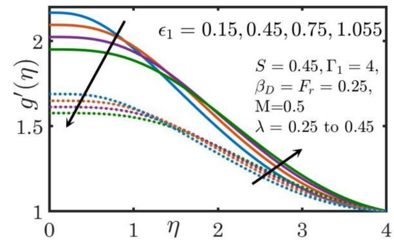

Figure 7. Impact of ε_1 and λ over g'.

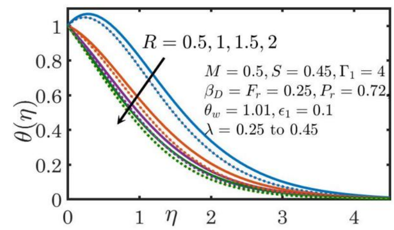

Figure 8. Influence for R and λ over temperature magnitudes.

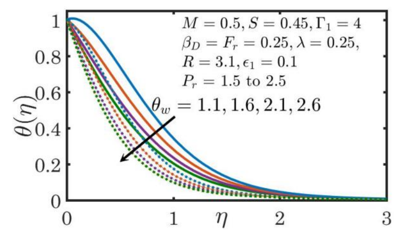

Figure 9. Impact for θ_w and P_r on temperature magnitudes.

temperature distribution. The reduction in temperature is observed as the P_r escalates for both linear and nonlinear surfaces in Figure 9. The thickness of the thermal boundary layer diminishes as the P_r increases. The P_r, which is the ratio of momentum-to-thermal diffusivity, is indicative of the heat transfer problem. The P_r has control over the overall thickening of the energy and thermal boundary layers in heat transfer problems. The thermal boundary layer for fluid metals is most likely thicker than the momentum boundary layer because heat diffuses more rapidly when the speed is low compared to the Prandtl number. In addition, lower Prandtl liquids possess higher thermal conductivities than higher liquids, which allows heat to diffuse through sheet at a faster rate. Therefore, the P_r can be utilized to hasten the cooling process. Additionally, as depicted in Figure 9, an escalation in θ_w diminishes the temperature function $\theta(\eta)$.

Figures 10 and 11 depict the concentration of species A and B, in relation to the proportion of momentum diffusivity to mass diffusivity $Sc_A = Sc_B = 0.5$, and strengths of homogeneous- heterogeneous reactions "$K_s = K_0 = 1.5$". It is recorded that $G(\eta)$ escalates as Sc_A and λ incremented, while $H(\eta)$ decreases for the same related parameters. Additionally, it is inferred that a rise in numeric for λ has an insignificant impact on $H(\eta = 0)$ and a significant impact over $G(\eta = 0)$. The figures depicted in Figures 12 and 13 illustrate the behavior of $G(\eta)$ and $H(\eta)$, as K_0 and K_s strengthen. The concentration $G(\eta)$ exhibits negligible decrease with K_0, which is only noticeable near the wall. On the other side, in close proximity to the wall, $G(\eta)$ experiences a significant decrease across K_s. Higher numeric for K_s and K_0 result in an elevation $H(\eta)$, as depicted in Figure 13. It is imperative to notice that an upsurge in numeric of K_s from 1.5 to 3.5 at all points of η within [0, 1.9] culminates in a substantial augmentation of $H(\eta)$ profile. Nevertheless, this substantial

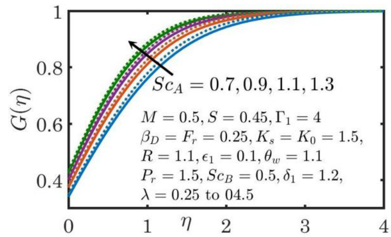

Figure 10. Influence of Sc_A and λ over $G(\eta)$.

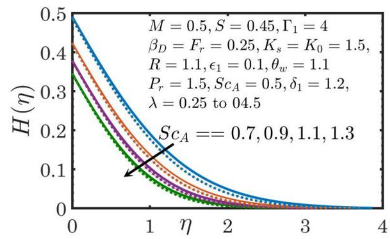

Figure 11. Influence of Sc_B and λ over $H(\eta)$.

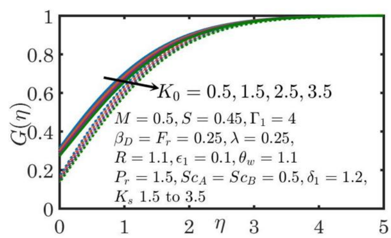

Figure 12. Influence of K_0 and K_s over $G(\eta)$.

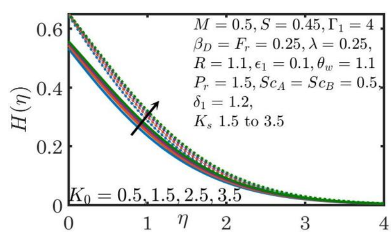

Figure 13. Influence of K_0 and K_s over $H(\eta)$.

increase decreases as K_s becomes larger. By enlarging values of δ_1 and K_s, gain an elevation and deceleration respectively over $H(\eta)$, as depicted in Figure 13. This noteworthy decrease can be ascribed to the magnitude designated to parameter δ_1 (Figure 14).

5. Concluding remarks

The primary aim of this work is to provide a mathematical methodology that utilizes numerical simulations to examine the impact of nonlinear thermal radiation and induced magnetic field on the flow behavior of a viscoelastic fluid toward a stagnation point in a non-Darcian permeable medium. The system of coupled non-linear differential equations is solved *via* the SRM approach

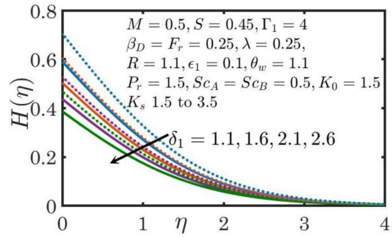

Figure 14. Influence of δ_1 and K_s over $H(\eta)$.

in order to get numerical solutions. The present technique is used to effectively tackle the governing equations of fluid flow as well as their associated boundary conditions. The acquired results are shown using visual representations, and a comparison is made between these findings and those of a prior study. The current investigation has produced numerous significant conclusions, which are outlined below:

i. The presence of parameter M leads to a decrease in both the magnitude and rate of change of induced magnetic fields.
ii. An upsurge in the parameter Γ_1 results in a decline in the velocity profiles.
iii. By enlarging the parameter S results in a deceleration of the flow in both $f'(\eta)$, and $g'(\eta)$.
iv. The velocity f^' (η) decreases across both parametric quantities of β_D and F_r.
v. The $g'(\eta)$ field experiences a decrease in proximity to the boundary, while increasing further away with an increase in ε_1.
vi. The $g'(\eta)$ experiences a reduction with an increase in λ within the vicinity of the wall. This is subsequently followed by a negligible increment.
vii. The $\theta(\eta)$ experiences a reduction with respect to both parameters i.e., with an increase in the magnitude of R and λ.
viii. The reduction in temperature is observed as the P_r and θ_w escalates.
ix. $G(\eta)$ increases for Sc_A and λ increase, while $H(\eta)$ decreases.
x. The concentration $G(\eta)$ exhibits negligible decrease with K_0, which is only noticeable near the wall. On the other side, near the wall, $G(\eta)$ experiences a significant decrease across K_s. Higher numeric of K_s and K_0 resulting in an elevation $H(\eta)$.
xi. Higher values of the strength in δ_1 result in a deceleration respectively over $H(\eta)$.
xii. The SRM model demonstrates remarkable accuracy and numerical robustness for solving nonlinear boundary value issues encountered in the field of multi-physical reactive magnetic rheological nano fluid coated materials processing on complex surfaces.

Disclosure statement

No potential conflict of interest was reported by the author(s).

ORCID

Anwar Shahid http://orcid.org/0000-0003-2702-6457
Muhammad Mubashir Bhatti http://orcid.org/0000-0002-3219-7579

References

[1] N. Sandeep, C. Sulochana and B. R. Kumar, "MHD boundary layer flow and heat transfer past a stretching/shrinking sheet in a nanofluid," *J. Nanofluids*, vol. 4, no. 4, pp. 512–517, Dec. 2015. DOI: 10.1166/jon.2015.1181.

[2] F. A. Zahor, R. Jain, A. O. Ali and V. G. Masanja, "Modeling entropy generation of magnetohydrodynamics flow of nanofluid in a porous medium: a review," *HFF*, vol. 33, no. 2, pp. 751–771, Jan. 2023. DOI: 10.1108/HFF-05-2022-0266.

[3] I. L. Animasaun, "Dynamics of unsteady MHD convective flow with thermophoresis of particles and variable Thermo-physical properties past a vertical surface moving through binary mixture," *OJFD*, vol. 05, no. 02, pp. 106–120, Jun. 2015. DOI: 10.4236/ojfd.2015.52013.

[4] I. L. Animasaun, "Double diffusive unsteady convective micropolar flow past a vertical porous plate moving through binary mixture using modified Boussinesq approximation," *Ain Shams Eng. J.*, vol. 7, no. 2, pp. 755–765, Jun. 2016. DOI: 10.1016/j.asej.2015.06.010.

[5] M. Kothandapani and J. Prakash, "Effects of thermal radiation parameter and magnetic field on the peristaltic motion of Williamson nanofluids in a tapered asymmetric channel," *Int. J. Heat Mass Transf.*, vol. 81, pp. 234–245, Feb. 2015. DOI: 10.1016/j.ijheatmasstransfer.2014.09.062.

[6] A. Wakif, Z. Boulahia, F. Ali, M. R. Eid and R. Sehaqui, "Numerical analysis of the unsteady natural convection MHD Couette nanofluid flow in the presence of thermal radiation using single and two-phase nanofluid models for cu–water nanofluids," *Int. J. Appl. Comput. Math.*, vol. 4, no. 3, pp. 81, Jun. 2018. DOI: 10.1007/s40819-018-0513-y.

[7] M. Yavuz, N. Sene and M. Yıldız, "Analysis of the influences of parameters in the fractional second-grade fluid dynamics," *Mathematics*, vol. 10, no. 7, pp. 1125, Apr. 2022. DOI: 10.3390/math10071125.

[8] N. Sene, "Second-grade fluid with Newtonian heating under Caputo fractional derivative: analytical investigations via Laplace transforms," *MMNSA*, vol. 2, no. 1, pp. 13–25, Jan. 2022. DOI: 10.53391/mmnsa.2022.01.002.

[9] A. S. Oke, "Coriolis effects on MHD flow of MEP fluid over a non-uniform surface in the presence of thermal radiation," *Int. Commun. Heat Mass Transf.*, vol. 129, no. 105695, pp. 105695, Dec. 2021. DOI: 10.1016/j.icheatmasstransfer.2021.105695.

[10] M. M. Bhatti and R. Ellahi, "Numerical investigation of non-Darcian nanofluid flow across a stretchy elastic medium with velocity and thermal slips," *Numer. Heat Transf. B Fundam.*, vol. 83, no. 5, pp. 323–343, May, 2023. DOI: 10.1080/10407790.2023.2174624.

[11] R. C. Bataller, "Viscoelastic fluid flow and heat transfer over a stretching sheet under the effects of a non-uniform heat source, viscous dissipation and thermal radiation," *Int. J. Heat Mass Transf.*, vol. 50, no. 15–16, pp. 3152–3162, Jul. 2007. DOI: 10.1016/j.ijheatmasstransfer.2007.01.003.

[12] V. Singh and S. Agarwal, "Heat transfer for two types of viscoelastic fluid over an exponentially stretching sheet with variable thermal conductivity and radiation in porous medium," *Therm. Sci.*, vol. 18, no. 4, pp. 1079–1093, Oct. 2014. DOI: 10.2298/TSCI111102144S.

[13] M. H. Abolbashari, N. Freidoonimehr, F. Nazari and M. M. Rashidi, "Analytical modeling of entropy generation for Casson nano-fluid flow induced by a stretching surface," *Adv. Powder Technol.*, vol. 26, no. 2, pp. 542–552, Mar. 2015. DOI: 10.1016/j.apt.2015.01.003.

[14] S. K. Adegbie, O. K. Kọrikọ and I. L. Animasaun, "Melting heat transfer effects on stagnation point flow of micropolar fluid with variable dynamic viscosity and thermal conductivity at constant vortex viscosity," *J. Nigerian Math. Soc.*, vol. 35, no. 1, pp. 34–47, Apr. 2016. DOI: 10.1016/j.jnnms.2015.06.004.

[15] N. Sandeep, C. Sulochana and I. L. Animasaun, "Stagnation-point flow of a Jeffrey nanofluid over a stretching surface with induced magnetic field and chemical reaction," *JERA*, vol. 20, pp. 93–111, Jan. 2015. DOI: 10.4028/www.scientific.net/JERA.20.93.

[16] E. H. Aly and I. Pop, "MHD flow and heat transfer near stagnation point over a stretching/shrinking surface with partial slip and viscous dissipation: hybrid nanofluid versus nanofluid," *Powder Technol.*, vol. 367, pp. 192–205, May, 2020. DOI: 10.1016/j.powtec.2020.03.030.

[17] W. Ibrahim and A. Tulu, "Magnetohydrodynamic (MHD) boundary layer flow past a wedge with heat transfer and viscous effects of nanofluid embedded in porous media," *Math. Probl. Eng.*, vol. 2019, pp. 1–12, Jan. 2019. DOI: 10.1155/2019/4507852.

[18] K. Ramesh, S. U. Khan, M. Jameel, M. I. Khan, Y.-M. Chu and S. Kadry, "Bioconvection assessment in Maxwell nanofluid configured by a Riga surface with nonlinear thermal radiation and activation energy," *Surf. Interfaces*, vol. 21, no. 100749, pp. 100749, Dec. 2020. DOI: 10.1016/j.surfin.2020.100749.

[19] R. Mohana Ramana, K. Venkateswara Raju and J. Girish Kumar, "Multiple slips and heat source effects on MHD stagnation point flow of Casson fluid over a stretching sheet in the presence of chemical reaction," *Mater. Today*, vol. 49, pp. 2306–2315, Jan. 2022. DOI: 10.1016/j.matpr.2021.09.348.

[20] M. M. Khader and M. M. Babatin, "Numerical study for improvement the cooling process through a model of Powell-Eyring fluid flow over a stratified stretching sheet with magnetic field," *Case Stud. Therm. Eng.*, vol. 31, pp. 101786, Mar. 2022. DOI: 10.1016/j.csite.2022.101786.

[21] S. Rehman, N. Muhammad, M. Alshehri, S. Alkarni, S. M. Eldin and N. A. Shah, "Analysis of a viscoelastic fluid flow with Cattaneo–Christov heat flux and Soret–Dufour effects," *Case Stud. Therm. Eng.*, vol. 49, no. 103223, pp. 103223, Sept. 2023. DOI: 10.1016/j.csite.2023.103223.

[22] J. H. Merkin, “A model for isothermal homogeneous-heterogeneous reactions in boundary-layer flow,” *Math. Comput. Model.*, vol. 24, no. 8, pp. 125–136, Oct. 1996. DOI: 10.1016/0895-7177(96)00145-8.

[23] F. Mabood, W. A. Khan and A. I. M. Ismail, “MHD stagnation point flow and heat transfer impinging on stretching sheet with chemical reaction and transpiration,” *Chem. Eng. J.*, vol. 273, pp. 430–437, Aug. 2015. DOI: 10.1016/j.cej.2015.03.037.

[24] M. Durairaj, S. Ramachandran and R. M. Mehdi, “Heat generating/absorbing and chemically reacting Casson fluid flow over a vertical cone and flat plate saturated with non-Darcy porous medium,” *HFF*, vol. 27, no. 1, pp. 156–173, Jan. 2017. DOI: 10.1108/HFF-08-2015-0318.

[25] I. L. Animasaun, “Effects of thermophoresis, variable viscosity and thermal conductivity on free convective heat and mass transfer of non-darcian MHD dissipative Casson fluid flow with suction and nth order of chemical reaction,” *J. Nigerian Math. Soc.*, vol. 34, no. 1, pp. 11–31, Apr. 2015. DOI: 10.1016/j.jnnms.2014.10.008.

[26] W. A. Khan and I. M. Pop, “Effects of homogeneous–heterogeneous reactions on the viscoelastic fluid toward a stretching sheet,” *J. Heat Transf.*, vol. 134, no. 6, pp. 064506, Jun. 2012. DOI: 10.1115/1.4006016.

[27] M. R. Eid, K. L. Mahny and A. F. Al-Hossainy, “Homogeneous-heterogeneous catalysis on electromagnetic radiative Prandtl fluid flow: darcy-Forchheimer substance scheme,” *Surf. Interfaces*, vol. 24, pp. 101119, Jun. 2021. DOI: 10.1016/j.surfin.2021.101119.

[28] H. Zahir, J. Akram, R. K., Alhefthi, R. Fatima, M. Inc, Mehnaz, and Mustafa Inc, “Effect of nonlinear thermal radiation and homogeneous-heterogeneous reactions on peristaltic propulsion of Johnson-Segalman fluid,” *Ain Shams Eng. J.*, 15, no.2, p. 102383, Jul. 2023. DOI: 10.1016/j.asej.2023.102383.

[29] M. Hassan, M. Marin, A. Alsharif and R. Ellahi, “Convective heat transfer flow of nanofluid in a porous medium over wavy surface,” *Phys. Lett. A*, vol. 382, no. 38, pp. 2749–2753, Sep. 2018. DOI: 10.1016/j.physleta.2018.06.026.

[30] M. Izadi, M. A. Sheremet and S. A. M. Mehryan, “Natural convection of a hybrid nanofluid affected by an inclined periodic magnetic field within a porous medium,” *Chin. J. Phys.*, vol. 65, pp. 447–458, Jun. 2020. DOI: 10.1016/j.cjph.2020.03.006.

[31] M. R. Eid and M. A. Nafe, “Thermal conductivity variation and heat generation effects on magneto-hybrid nanofluid flow in a porous medium with slip condition,” *Waves Random Complex Media*, vol. 32, no. 3, pp. 1103–1127, May, 2022. DOI: 10.1080/17455030.2020.1810365.

[32] Z. Ying, B. He, L. Su and Y. Kuang, “Thermo-hydraulic analyses of the absorber tube with molten salt-based nanofluid and porous medium inserts,” *Sol. Energy*, vol. 226, pp. 20–30, Sept. 2021. DOI: 10.1016/j.solener.2021.08.021.

[33] K. Loganathan, N. Alessa, K. Tamilvanan and F. S. Alshammari, “Significances of Darcy–Forchheimer porous medium in third-grade nanofluid flow with entropy features,” *Eur. Phys. J. Spec. Top.*, vol. 230, no. 5, pp. 1293–1305, Jul. 2021. DOI: 10.1140/epjs/s11734-021-00056-6.

[34] N. Shah, P. Dhar, S. K. Chinige, M. Geier and A. Pattamatta, “Cascaded collision lattice Boltzmann model (CLBM) for simulating fluid and heat transport in porous media,” *Numer. Heat Transf. B Fundam.*, vol. 72, no. 3, pp. 211–232, Sept. 2017. DOI: 10.1080/10407790.2017.1377530.

[35] A. A. Alaidrous and M. R. Eid, “3-D electromagnetic radiative non-Newtonian nanofluid flow with Joule heating and higher-order reactions in porous materials,” *Sci. Rep.*, vol. 10, no. 1, pp. 14513, Sept. 2020. DOI: 10.1038/s41598-020-71543-4.

[36] M. Irfan, “Study of Brownian motion and thermophoretic diffusion on non-linear mixed convection flow of Carreau nanofluid subject to variable properties,” *Surf. Interfaces*, vol. 23, no. 100926, pp. 100926, Apr. 2021. DOI: 10.1016/j.surfin.2021.100926.

[37] M. R. Eid, “Thermal characteristics of 3D nanofluid flow over a convectively heated Riga surface in a Darcy–Forchheimer porous material with linear thermal radiation: an optimal analysis,” *Arab. J. Sci. Eng.*, vol. 45, no. 11, pp. 9803–9814, Nov. 2020. DOI: 10.1007/s13369-020-04943-3.

[38] M. M. Bhatti, H. F. Öztop and R. Ellahi, “Study of the magnetized hybrid nanofluid flow through a flat elastic surface with applications in solar energy,” *Materials (Basel)*, vol. 15, no. 21, pp. 7507, Oct. 2022. DOI: 10.3390/ma15217507.

[39] S. E. Ahmed, A. A. M. Arafa, S. A. Hussein and Z. Morsy, “Time-dependent squeezing flow of variable properties ternary nanofluids between rotating parallel plates with variable magnetic and electric fields,” *Numer. Heat Transf. A*, pp. 1–30, Oct. 2023. DOI: 10.1080/10407782.2023.2272292.

[40] M. B. Arain, A. Zeeshan, M. M. Bhatti, M. S. Alhodaly and R. Ellahi, “Description of non-Newtonian bio-convective Sutterby fluid conveying tiny particles on a circular rotating disk subject to induced magnetic field,” *J. Cent. South Univ.*, vol. 30, no. 8, pp. 2599–2615, Aug. 2023. DOI: 10.1007/s11771-023-5398-1.

[41] F. M. Ali, R. Nazar, N. M. Arifin and I. Pop, “MHD stagnation-point flow and heat transfer towards stretching sheet with induced magnetic field,” *Appl. Math. Mech.-Engl. Ed.*, vol. 32, no. 4, pp. 409–418, Apr. 2011. DOI: 10.1007/s10483-011-1426-6.

[42] L. N. Trefethen, *Spectral Methods in MATLAB*. Philadelphia, PA: Society for Industrial and Applied Mathematics, 2000,

[43] I. L. Animasaun, C. S. K. Raju and N. Sandeep, "Unequal diffusivities case of homogeneous–heterogeneous reactions within viscoelastic fluid flow in the presence of induced magnetic-field and nonlinear thermal radiation," *Alex. Eng. J.*, vol. 55, no. 2, pp. 1595–1606, Jun. 2016. DOI: 10.1016/j.aej.2016.01.018.